water

MDPI

Article

Enhancement in Sulfamethoxazole Degradation via Efficient Heterogeneous Activation of Peracetic Acid by FeS

Linyi Li [1], Yanlin Wu [2,*] and Wenbo Dong [1,3,*]

[1] Shanghai Key Laboratory of Atmospheric Particle Pollution and Prevention, Department of Environmental Science & Engineering, Fudan University, Shanghai 200433, China; 20210740009@fudan.edu.cn
[2] School of Resources and Environmental Engineering, Shanghai Polytechnic University, Shanghai 201209, China
[3] Shanghai Institute of Pollution Control and Ecological Security, Shanghai 200092, China
* Correspondence: wuyanlin@fudan.edu.cn (Y.W.); wbdong@fudan.edu.cn (W.D.)

Abstract: Peracetic acid (PAA) has attracted increasing attention in wastewater decontamination for yielding reactive oxygen species (ROS). In this study, mackinawite (FeS) was synthesized and applied as the heterogeneous catalyst for PAA activation. Using sulfamethoxazole (SMX) as the target pollutant, the influences of FeS dosage, PAA dosage and initial pH values on SMX degradation by the FeS/PAA process were investigated. Under optimal conditions, SMX could be completely removed within 5 min with the apparent first-order rate constant (k_{obs}) of 7.71 × 10^{-4} s^{-1}. Electron spin resonance spectroscopy (ESR) analysis and radical scavenging experiments were modulated to detect the active species. During the activation process of PAA, various active components were evidenced to be hydroxyl radicals ($HO^{\bullet}$), singlet oxygen ($^1O_2$), superoxide radicals ($O_2^{\bullet-}$) and organic radicals ($R\text{-}O^{\bullet}$, e.g., $CH_3C(O)O^{\bullet}$ and $CH_3C(O)OO^{\bullet}$), whereas $HO^{\bullet}$ and $R\text{-}O^{\bullet}$ were demonstrated as the dominant active species responsible for SMX abatement. Both dissolved Fe(II) ions and active sites on the surface of FeS were proven to be activators for PAA, and SMX abatement was highly promoted as a result. Furthermore, the acidic pH displayed superior efficiency in SMX decomposition compared with alkaline and neutral conditions. Five degradation pathways of SMX were put forward and the toxicity of byproducts was further evaluated. Overall, this study provided an efficient and environmentally friendly PAA activation approach using FeS, which might broaden its applicability in the remediation of micropollutants.

Keywords: FeS; peracetic acid; free radicals; mechanism; removal pathways

Citation: Li, L.; Wu, Y.; Dong, W. Enhancement in Sulfamethoxazole Degradation via Efficient Heterogeneous Activation of Peracetic Acid by FeS. *Water* **2024**, *16*, 2405. https://doi.org/10.3390/w16172405

Academic Editor: Christos S. Akratos

Received: 6 August 2024
Revised: 21 August 2024
Accepted: 23 August 2024
Published: 27 August 2024

1. Introduction

Advanced oxidation processes (AOPs) have been widely used for the treatment of recalcitrant organic wastewater containing hazardous organics such as pesticides, dyes and antibiotics, exhibiting a promising application prospect [1,2]. Peracetic acid ($CH_3C(O)OOH$, PAA), as an organic peracid with poor solubility, has attracted increasing attention in AOPs [3]. Possessing robust oxidation capability due to high redox potential (1.06–1.96 V), PAA has been utilized as a disinfectant in fields like textiles, aquaculture and food processing for the past few decades [3–5]. Previous studies revealed that the concentrations and toxicities of the disinfection byproducts (DBPs) generated during the disinfection process with PAA were lower than those associated with traditional chlorine disinfection methods, well validating the safety of PAA for disinfection [6,7]. Moreover, PAA exhibited a lower bond energy for O-O bond (159 kJ mol^{-1}) than that of commonly used oxidants, such as hydrogen peroxide (H_2O_2, 213 kJ mol^{-1}) and peroxymonosulfate (PMS, 377 kJ mol^{-1}) [3,8–10]. Thus, the O-O bond of PAA was more easily decomposed with the generation of reactive oxygen species (ROS) including hydroxyl radicals ($HO^{\bullet}$), acetoxyl radicals ($CH_3C(O)O^{\bullet}$), and acetylperoxyl radicals ($CH_3C(O)OO^{\bullet}$) [11–14].

Various strategies, including ultraviolet (UV) [7,15], carbonaceous material [3] and transition metals [16,17], were widely developed as activators of PAA. UV was firstly employed in PAA activation for the degradation of naproxen (NPX), but with low efficiency and complex operation. Although powdered activated carbon (PAC) benefited contaminant removal, its practical application was restricted due to high production costs. Nevertheless, activation by transition metals (iron, cobalt, copper, etc.) has received widespread attention for its high efficiency, economic strengths, wide potential applications, etc. The catalytic performance of $CuCo_2O_4$-assisted PAA activation was greatly enhanced, but the tedious preparation process remained an issue. As one of the most widely distributed transition metals, iron has gained more favor due to its environmental friendliness and lack of energy consumption. For instance, the efficient abatement of contaminants such as NPX and bisphenol A (BPA) was found in the Fe(II)/PAA homogeneous system [18]. Despite this, the practical application of homogeneous systems was hindered in aspects such as strict pH requirements, slow Fe(III)/Fe(II) cycle conversion and the secondary pollution of iron precipitation. It was reported that iron-based solid-phase materials (zero-valent iron (nZVI), iron oxides, iron sulfides, etc.) had emerged as primary alternatives to Fe(II) owing to the inherent stability of the iron source within their internal structures [19–21]. As reported previously, the activation effect of nZVI was significant among these heterogeneous iron-based materials. However, due to the limitation of the proton transfer rate in the passivation layer, the release of Fe(II) into the aqueous solution was slowed, preventing continuous activation. Therefore, efforts should be made to find efficient, low-cost and environmentally friendly heterogeneous materials for PAA activation to promote the practical application of PAA-based processes.

As the main components of mackinawite, iron sulfide (FeS) is one kind of common iron mineral, extensively present in soil environments and initially extensively employed for dehalogenation and the reduction of Cr(VI) [22]. Previous studies revealed that serving as an electron donor, FeS exhibited robust reducing capabilities. Moreover, it demonstrated better adaptability to pH variations, making it commonly employed for the activation of H_2O_2, PMS and peroxydisulfate (PS) to efficiently degrade micropollutants [19,23,24]. Taking PMS as an example, the generation process of ROS was summarized in Equations (1)–(4). Furthermore, Fan et al. [25] discovered that in addition to the slow release of Fe(II), the Fe(III)/Fe(II) cycle could be accelerated by sulfur species on the FeS surface in the FeS/PS system (Equation (5)). As a corollary, PAA might also be activated by FeS, thereby rapidly degrading pollutants. Nevertheless, there have been few reports on the activation of novel oxidants such as PAA, though the utilization of FeS in PAA activation appeared to be potentially effective and held promise for contaminant decomposition. Moreover, previous studies have presented pyrite or pyrite tailings (FeS_2), another kind of common iron sulfide, as an effective catalyst for PAA activation [26,27]. For instance, Xing et al. [26] found that $CH_3C(O)OO^{\bullet}$ was the main radical generated from the pyrite/PAA system responsible for tetracycline (TC) abatement, and Fe(II) regeneration was boosted by the superior electron-donating ability of sulfur sites. However, these studies mainly focused on the identification of ROS in reaction systems, though there was still no closed-loop discussion on the main location of the reaction (which mainly occurred in aqueous solution or on the surface of solid catalyst), or on the ecotoxicity of the degradation byproducts of the target pollutant.

Considering the discussion above, sulfamethoxazole (SMX), as a representative substance of sulfonamide antibiotics, has been frequently detected in various environmental samples and water bodies such as surface water [28,29], rivers [30] and drinking water [31]. SMX was therefore selected as the target micropollutant. The aim of this study was to investigate the degradation capability and mechanisms of the FeS/PAA system towards SMX. FeS was successfully synthesized via the co-precipitation method confirmed by a series of characterization methods. Firstly, various catalysts and oxidizing agents were investigated. In addition, the elimination performance of FeS/PAA system was evaluated based on different operation parameters, including reactant dosages, initial pH values, and water matrices. Subsequently, both ESR and quenching experiments were performed to

determine the ROS by the process. The active reaction sites were explored and the mechanism of FeS for PAA activation was proposed. Finally, possible degradation pathways of SMX and the toxicity before and after treatment were estimated based on experiments and calculations.

$$Fe(III) + HSO_5^- \rightarrow Fe(II) + SO_5^{\bullet -} + H^+ \quad (1)$$

$$Fe(II) + HSO_5^- \rightarrow Fe(III) + SO_4^{\bullet -} + OH^- \quad (2)$$

$$Fe(II) + HSO_5^- \rightarrow Fe^{VI}O^{2+} + SO_4^{2-} + H^+ \quad (3)$$

$$SO_4^{\bullet -} + H_2O \rightarrow SO_4^{2-} + HO^{\bullet} + H^+ \quad (4)$$

$$S^{2-} + Fe(III) + 4H_2O \rightarrow Fe(II) + SO_4^{2-} + 8H^+ \quad (5)$$

2. Materials and Methods

2.1. Chemicals

Detailed information regarding chemicals and reagents used in this experiment is provided in Supplementary Materials, Text S1.

2.2. Preparation of FeS and PAA Solution

FeS was synthesized employing a modified co-precipitation method [32]. First, $FeSO_4 \cdot 7H_2O$ and $Na_2S \cdot 9H_2O$ were mixed with 1:1 molar ratio and then stood for 4 h. Subsequently, the obtained precipitate was rinsed several times with ultrapure water to remove excess dissolved salt ions and dried in a vacuum freeze dryer for 24 h. The resulting products were stored in a desiccator for later use. Based on a series of comprehensive characterization analyses, FeS synthesized by the homogeneous precipitation method was found to be rough and porous, and the fundamental chemical composition was found to be consistent with references in the literature, confirming the successful synthesis of FeS (particularly discussed in Text S2).

PAA was prepared according to a previous study [33,34]. Briefly, PAA test solution was obtained from co-heating of CH_3COOH and H_2O_2 with concentrated H_2SO_4 as a catalyst, and the principle of this reaction is illustrated in Equation (6). The details are appended in Text S3. In addition, the concentration of total peroxides (containing both PAA and H_2O_2) and H_2O_2 in the stock solution was determined with the iodometric method and permanganate titration, respectively (Texts S4 and S5) [4,34]. In the freshly prepared PAA solution, the molar ratio of PAA to H_2O_2 was approximately 10:1. Notably, the PAA and H_2O_2 of the test solution needed to be calibrated periodically due to the reversible reaction (Equation (6)).

$$CH_3COOH + H_2O_2 \rightarrow CH_3C(O)OOH + H_2O \quad (6)$$

2.3. Experimental Procedure

The batch experiments were carried out in a 150 mL beaker with continuous magnetic stirring at an ambient temperature of 25 ± 2 °C. Reactions were initiated by adding PAA to a 100 mL solution containing SMX and FeS. The dosages of FeS and PAA were controlled according to the experimental conditions. In experiments investigating the effects of initial pH on SMX degradation, diluted $HClO_4$ (0.1 mol·L^{-1}) and NaOH (0.1 mol·L^{-1}) were applied to adjust the initial pH required for the experiment with no buffer employed. However, the adjustment of pH in the actual water treatment process required manpower and financial resources. In addition to experiments exploring the influences of pH, most of the experiments were performed at pH 5.5 (without adjustment). As the reaction proceeded, about 1 mL solution was extracted by syringe at predetermined time intervals. The extracted solution was passed through a filter membrane with a pore size of 0.22 μm, and 700 μL of the solution was immediately mixed with 100 μL of 100 mmol·L^{-1} $Na_2S_2O_3$ to terminate the reaction prior to analysis. All degradation experiments were repeated

at least twice, and the displayed data were accompanied with error bars to indicate the variability.

2.4. Analytical Methods

The microscopic surface morphology and structural parameters (specific surface area, pore size, etc.) were characterized by scanning electron microscope (SEM) and micropore chemisorption analyzer, respectively. The surface elemental composition and valence states of FeS were analyzed by X-ray photoelectron spectroscopy (XPS). The crystallinity and internal structure were investigated using X-Ray Diffraction (XRD). The concentration of SMX was quantitatively detected by high-performance liquid chromatography (HPLC). The detection of Fe(II) concentration was determined by the ferrozine method [35] with a UV–vis spectrophotometer. The ROSs were recognized through electron spin-resonance spectroscopy (ESR) with DMPO/TEMP/DIPPMPO as spin trapping agents. The degradation intermediate compounds of SMX were measured by the LC-MS/MS system. The detailed instruments, characterization methods and software parameters are summarized in Table S1 and Text S6.

2.5. Computational Methods

The Gaussian 09W suite of software was employed for density functional theory (DFT) calculations [36], and then the imaged results were plotted from the Multifunctional wavefunction analyzer (Multiwfn 3.8) [37] and Visual Molecular Dynamics (VMD 1.9.3) program [38]. Furthermore, the acute and chronic toxicity of SMX and its reaction intermediates were predicted by using the Ecological Structure Activity Relationships (ECOSAR 2.2) program [39]. The detailed procedure and software parameters are listed in Texts S7 and S8.

3. Results and Discussions

3.1. Activation of PAA by Various Activators for the Degradation of SMX

Five activators (FeS, CuS, Fe_3O_4, CuO, Co_3O_4) were tested for SMX removal resulting from PAA activation. As illustrated in Figure 1, SMX underwent remarkable decomposition by the FeS/PAA process. Control experiments showed that the SMX was almost non-degradable in the presence of PAA. The results indicated that SMX was hardly degraded by PAA without any activator. The concentration of SMX remained stable when FeS was added alone, which revealed that the adsorption of SMX by FeS itself could be neglected. In comparison, slight or negligible abatement of SMX could be found in other PAA activation systems within 5 min, indicating that the adsorption onto CuS, Fe_3O_4, CuO and Co_3O_4 could be excluded at a comparatively low dosage. This might be due to the concentration and time scale of this paper. If these activators were mainly deactivated by mass transfer on the surface or the active site, the activation efficiency of PAA could be relatively slow, and PAA activation might not be predicted by judging the degradation of SMX within a time scale of 5 min. It could be concluded that the FeS/PAA system achieved the complete removal of SMX within 5 min, confirming the feasibility of utilizing FeS to construct a heterogeneous system for activating PAA to degrade SMX. FeS could achieve significant destruction efficiency even at an extremely low dosage and much shorter reaction time.

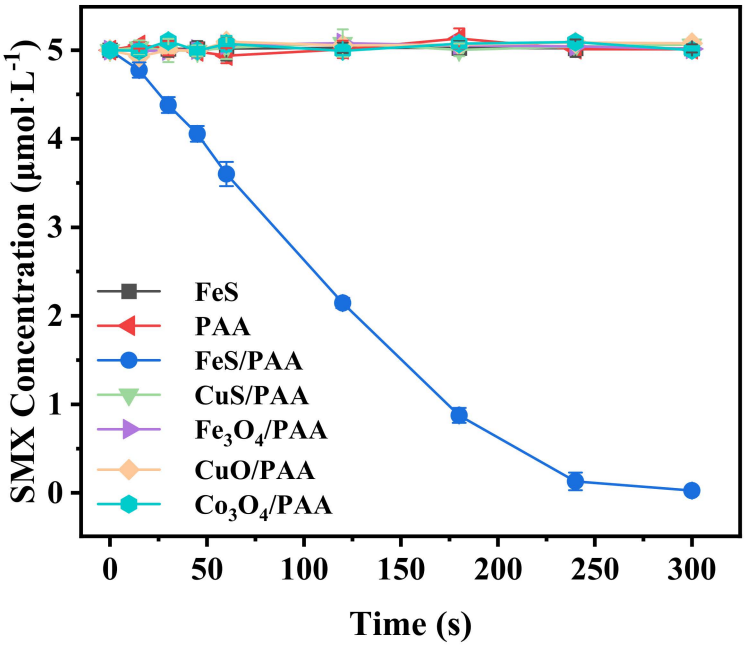

Figure 1. Effect of different activators on SMX degradation. Experimental conditions: $[SMX]_0$ = 5 μmol·L^{-1}, $[FeS]_0$ = $[CuS]_0$ = $[Fe_3O_4]_0$ = $[CuO]_0$ = $[Co_3O_4]_0$ = 50 mg·L^{-1}, $[PAA]_0$ = 200 μmol·L^{-1}, pH = 5.5.

3.2. Activation of Various Oxidants by FeS for the Degradation of SMX

Five oxidants (PAA, PMS, PS, H_2O_2, PI) were tested for SMX removal resulting from the activation by FeS. It could be observed from Figure 2 that the degradation rates of SMX by FeS/PS and FeS/PMS systems were 9.44% and 94.37%, respectively, with corresponding kobs values of 5.99 × 10^{-3} s^{-1} and 1.82 × 10^{-4} s^{-1}. Nevertheless, contrary to the remarkable oxidation of bisphenol AF (BPAF) reported by Wang et al. [19], the FeS/PI system was unable to remove SMX under the given conditions. On the one hand, the dosage of FeS and PAA adopted in this paper ($[FeS]_0$ = 50 mg·L^{-1}, $[PAA]_0$ = 200 μmol·L^{-1}) was far below that used in previous research ($[FeS]_0$ = 1 g·L^{-1}, $[PI]_0$ = 1 mmol·L^{-1}). On the other hand, the difference could be attributed to the short reaction time, which might not have fully demonstrated the oxidative capability of the selected system. Overall, the FeS/PAA system demonstrated excellent abatement efficiency compared to any other oxidant process activated by FeS.

According to the literature, the complete degradation of 2,4-dichlorophenoxyacetic acid could be achieved within 300 min based on the FeS/H_2O_2 system [40]. Due to the presence of trace amounts of H_2O_2 in the prepared PAA solution ([PAA]:[H_2O_2] = 10:1), H_2O_2 in the system might be activated by FeS to generate ROS, thus degrading SMX. Following the results of control experiments, even when increasing the H_2O_2 concentration to 200 μmol·L^{-1}, there was no reduction in the concentration of SMX (Figures 2 and S4), indicating that the influence of H_2O_2 on the degradation of SMX in the system could be ruled out. In terms of the FeS/PMS system, the FeS-activated PMS reaction was carried out at the surface of FeS with the production of ROS. Based on structural similarities (O-O bond) between PAA and PMS [41,42], it could be inferred that the process of FeS activating PAA was similar to that of PMS (primarily discussed in Section 3.6). However, it should be addressed that compared to PMS, PAA presented the advantage of lower ecological toxicity, making it more advantageous with regard to safety for practical applications [43].

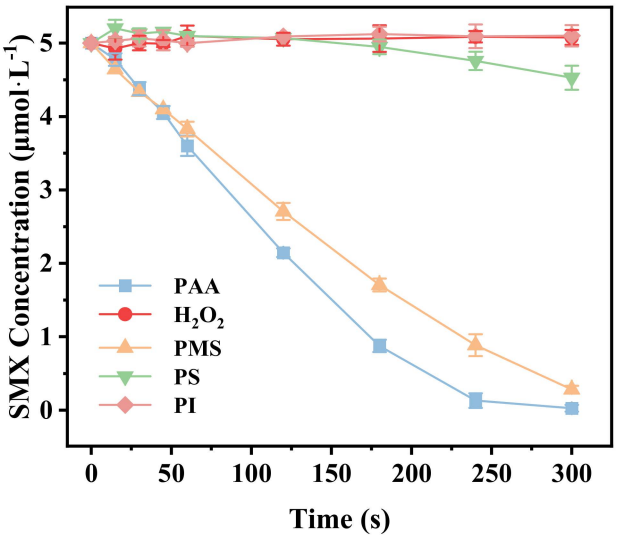

Figure 2. Effect of different oxidants on SMX degradation. Experimental conditions: $[SMX]_0$ = 5 μmol·L^{-1}, $[FeS]_0$ = 50 mg·L^{-1}, $[PAA]_0$ = $[PMS]_0$ = $[PS]_0$ = $[PI]_0$ = $[H_2O_2]_0$ = 200 μmol·L^{-1}, pH = 5.5.

3.3. Effect of Reagent Dosage on SMX Degradation

To evaluate the effect of FeS dosage (25–100 mg·L^{-1}), parallel experiments were performed by adding FeS to the reaction solution. With the PAA concentration fixed at 200 μmol·L^{-1}, the degradation rate of SMX was significantly improved as the FeS dosage increased from 25 mg·L^{-1} to 50 mg·L^{-1} (Figure 3a), accompanied by the corresponding increase in k_{obs} from 3.24 × 10^{-3} s^{-1} to 7.71 × 10^{-3} s^{-1} (Figure S5a). Upon further increasing the FeS dosage to 100 mg·L^{-1}, SMX was completely removed in 2 min, with a k_{obs} of 1.43 × 10^{-2} s^{-1}. On the one hand, PAA activation could be enhanced by more active sites on the surface of higher FeS dosage. On the other hand, this change could be explained by the higher concentration of dissolved Fe(II) with the increasing FeS dosage in the reaction system (mainly discussed in Section 3.6). Considering the balance between the degradation efficiency of SMX and experimental operability, an FeS dosage of 50 mg·L^{-1} was adopted in this paper.

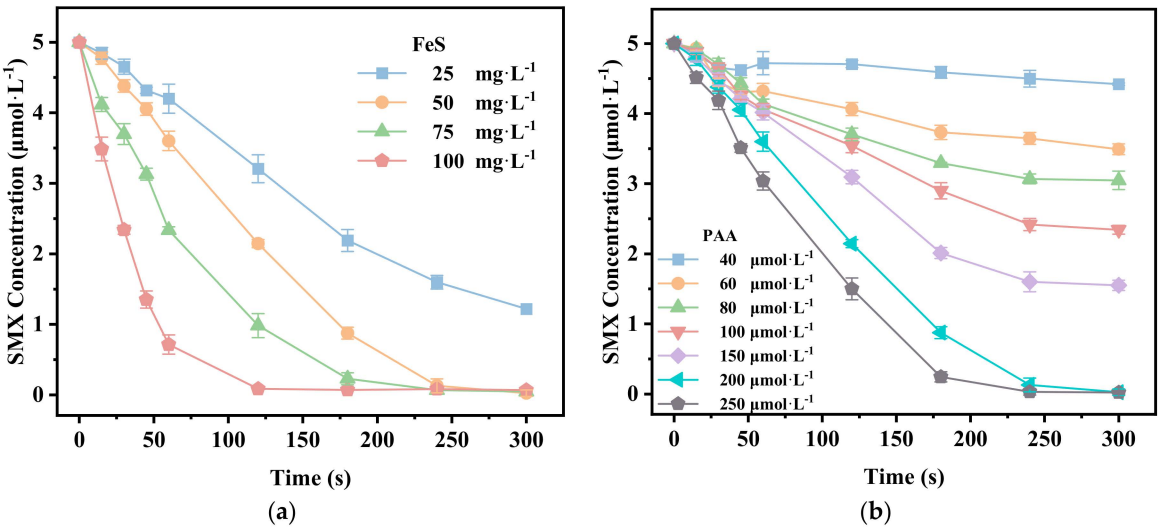

Figure 3. Effect of (**a**) FeS dosage and (**b**) PAA concentration on SMX degradation in FeS/PAA system. Experimental conditions for (**a**): $[SMX]_0$ = 5 μmol·L^{-1}, $[PAA]_0$ = 200 μmol·L^{-1}, pH = 5.5; for (**b**): $[SMX]_0$ = 5 μmol·L^{-1}, $[FeS]_0$ = 50 mg·L^{-1}, pH = 5.5.

In the FeS/PAA system, PAA served as the primary source of ROS [44], and its concentration must be taken into consideration. The effect of different concentrations of PAA varying from 40 to 250 μmol·L^{-1} on the degradation of SMX is presented in Figure 3b. When the PAA concentration ranged from 40 μmol·L^{-1} to 250 μmol·L^{-1}, the degradation of SMX was significantly enhanced, with the corresponding k_{obs} going from 4.78 × 10^{-4} s^{-1} to 9.93 × 10^{-3} s^{-1} (Figure S5b). In other words, under the current experimental conditions, the self-clearing effect caused by excessive PAA hardly occurred in the FeS/PAA process (Equations (7) and (8)) [6]. Considering degradation efficiency and environmental friendliness, the PAA concentration was set at 200 μmol·L^{-1} in subsequent experiments.

The effect of the concentration of SMX, the model pollutant, was also investigated. As illustrated in Figure S6, SMX with a lower concentration could be completely removed by the FeS/PAA system. While the concentration of SMX was raised to 20 μmol·L^{-1}, the corresponding k_{obs} decreased from to 7.71 × 10^{-3} s^{-1} to 4.94 × 10^{-3} s^{-1}. This could be attributed to insufficient ROS production for rapid SMX abatement. In order to satisfy the limit of detection and simultaneously simulate the actual environment as much as possible, 5 μmol·L^{-1} of SMX was adopted in this paper.

$$CH_3C(O)OOH + HO^{\bullet} \rightarrow CH_3C(O)OO^{\bullet} + H_2O \quad (7)$$

$$CH_3C(O)OOH + CH_3C(O)O^{\bullet} \rightarrow CH_3C(O)OO^{\bullet} + CH_3C(O)OH \quad (8)$$

3.4. Effect of Initial pH on SMX Degradation

pH was also a key factor worthy of being taken into account, and thus the degradation of SMX with different initial pH conditions was also investigated. From Figure S8, the pH changed over a limited range during the reactions when the initial pH of the selected system was controlled at 3.0, 4.0, 8.0, 9.0 and 10.0. However, probably due to rapid consumption of PAA, the pH value quickly decreased to 4.1–4.3 after the reaction of 60 s in the systems with initial pH values of 5.5, 6.0 and 7.0. As shown in Figures 4 and S7, the SMX degradation efficiency was decreased when the pH increased from 3.0 to 7.0, and the k_{obs} decreased from 1.91 × 10^{-2} s^{-1} to 2.30 × 10^{-3} s^{-1} correspondingly, which aligned with the conclusions of PI activation by FeS [19]. Nonetheless, in an alkaline environment with pH > 7, the removal efficiency for SMX sharply declined, indicating the poor applicability of the system in alkaline conditions. This result required further analysis and discussion from the perspectives of radical oxidation ability, and the chemical forms of reactants.

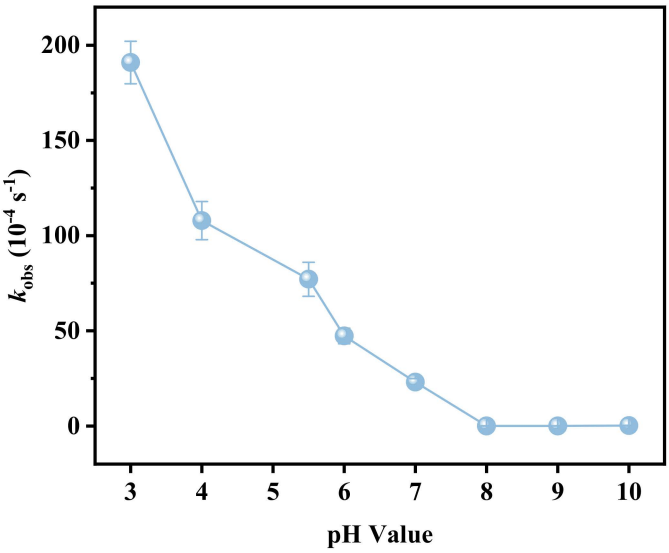

Figure 4. Effects of initial pH values on corresponding degradation rate constants in FeS/PAA system. Experimental conditions: $[SMX]_0$ = 5 μmol·L^{-1}, $[FeS]_0$ = 50 mg·L^{-1}, $[PAA]_0$ = 200 μmol·L^{-1}.

The oxidation ability of radicals influenced by the surrounding pH value was a key factor affecting SMX degradation. In terms of $HO^{\bullet}$, the oxidation capacity of $HO^{\bullet}$ would decrease (2.7 V in acidic solution and 1.8 V in neutral solution) as the pH increased [45,46]. The morphology of reactants was also an important factor affecting SMX degradation. Figure S9 depicts the distribution of PAA under different pH conditions and it could be observed that the pK_a value of PAA was 8.2 (Equations (9)–(11)), suggesting that when the pH exceeded 8.2, PAA predominantly existed in the form of negative ions (PAA^-) [47]. However, studies have shown that compared with PAA^-, the neutral form of PAA was more prone to accept the electron from the catalyst for activation and possessed stronger oxidizing capacity on account of a higher oxidation potential (E_0 (PAA) = 1.96V, E_0 (PAA^-) = 1.01V) [48–50]. In addition to the oxidizing ability, PAA^- might react more easily with some ROS (e.g., $k_{PAA-,HO\bullet} = 9.97 \times 10^9$ $mol^{-1} \cdot s^{-1}$, $k_{PAA0,HO\bullet} = 9.33 \times 10^8$ $mol^{-1} \cdot s^{-1}$) [44]. This was the reason why the higher degradation efficiency of the FeS/PAA system for SMX could be reached under acidic and neutral conditions.

FeS was the primary component for PAA activation. Under a lower-pH environment, higher Fe(II) concentration leached from FeS was favorable for enhancing the homogeneous activation process of PAA in the aqueous solution. Simultaneously, the generated Fe(III) could be fixed in the structural spaces of FeS, reducing the precipitation of Fe(II) and promoting the sustained generation of ROS in the reaction system, which ultimately enhanced the degradation capability of SMX. Notably, the chemical form of iron transitioned from Fe(III) to $Fe(OH)^{2+}$ (peaking at pH = 6.5) within the pH range of 3.0–6.5, and it was likely to be the most reactive among the iron species according to research [51]. Nevertheless, the trend observed in this paper, where SMX degradation efficiency improved as the reaction system became more acidic, indicates the need for a comprehensive consideration of various factors.

Overall, it could be concluded that the pH range for the SMX oxidation of the FeS/PAA heterogeneous system was expanded from strictly limited to pH = 2.0–4.0 to pH = 7.0, indicating an improved adaptability to pH.

$$CH_3C(O)OOH + H_2O \rightarrow CH_3C(O)OO^- + H_3O^+ \quad (9)$$

$$CH_3C(O)OOH + CH_3C(O)OO^- \rightarrow CH_3C(O)OH + CH_3C(O)O^- + O_2 \quad (10)$$

$$CH_3C(O)OO^- + H_2O_2 \rightarrow CH_3C(O)O^- + H_2O + O_2 \quad (11)$$

3.5. Identification of the Main Reactive Oxygen Species

Studies have shown that ROSs are crucial in the degradation of micropollutants [52]. The process of PAA activation might produce a variety of ROS, including $HO^{\bullet}$, $O_2^{\bullet -}$, $^1O_2$ and so on. In order to have a better understanding of the ROSs involved in the degradation process of SMX, electron spin resonance spectroscopy (ESR) and selective quenching experiments were performed.

Biological spin trapping reagents like 5,5-dimethyl-pyrroline-N-oxide (DMPO) were introduced into the solution to prolong the lifespan of ROSs, which therefore could be visualized by ESR spectra [53]. Typical signals of DMPO-$HO^{\bullet}$, DMPO-$O_2^{\bullet -}$ and TEMP-$^1O_2$ were obtained in Figure 5a–c. Based on the relative intensities, $HO^{\bullet}$ was the primary radical. As reported in previous studies [54,55], phosphorylated spin trap 5-diisopropoxyphosphoryl-5-methyl-1-pyrroline N-oxide (DIPPMPO) could simultaneously capture both $HO^{\bullet}$ and carbon-centered radicals ($CH_3^{\bullet}$), which could be distinguished by the presence or absence of tert-butanol (TBA). Since R-$O^{\bullet}$ could decompose into $CH_3^{\bullet}$ [55], the detected characteristic peak of $CH_3^{\bullet}$ indirectly confirmed the generation of R-$O^{\bullet}$. To ascertain the production of R-$O^{\bullet}$ in the FeS/PAA system, ESR spectra were also recorded in the presence and absence of TBA. As shown in Figure 5d, the addition of TBA to the system led to the disappearance of the adduct signal of DMPO-$HO^{\bullet}$ and the appearance of the characteristic

peak of DMPO-$CH_3^{\bullet}$; thus, the formation of R-$O^{\bullet}$ in the selected system was verified (Equations (12)–(14)).

$$CH_3C(O)OOH + Fe(II) \rightarrow CH_3C(O)O^- + Fe(III) + HO^{\bullet} \quad (12)$$

$$CH_3C(O)OOH + Fe(II) \rightarrow CH_3C(O)O^{\bullet} + Fe(III) + OH^- \quad (13)$$

$$CH_3C(O)OOH + HO^{\bullet} \rightarrow CH_3C(O)^{\bullet} + H_2O + O_2 \quad (14)$$

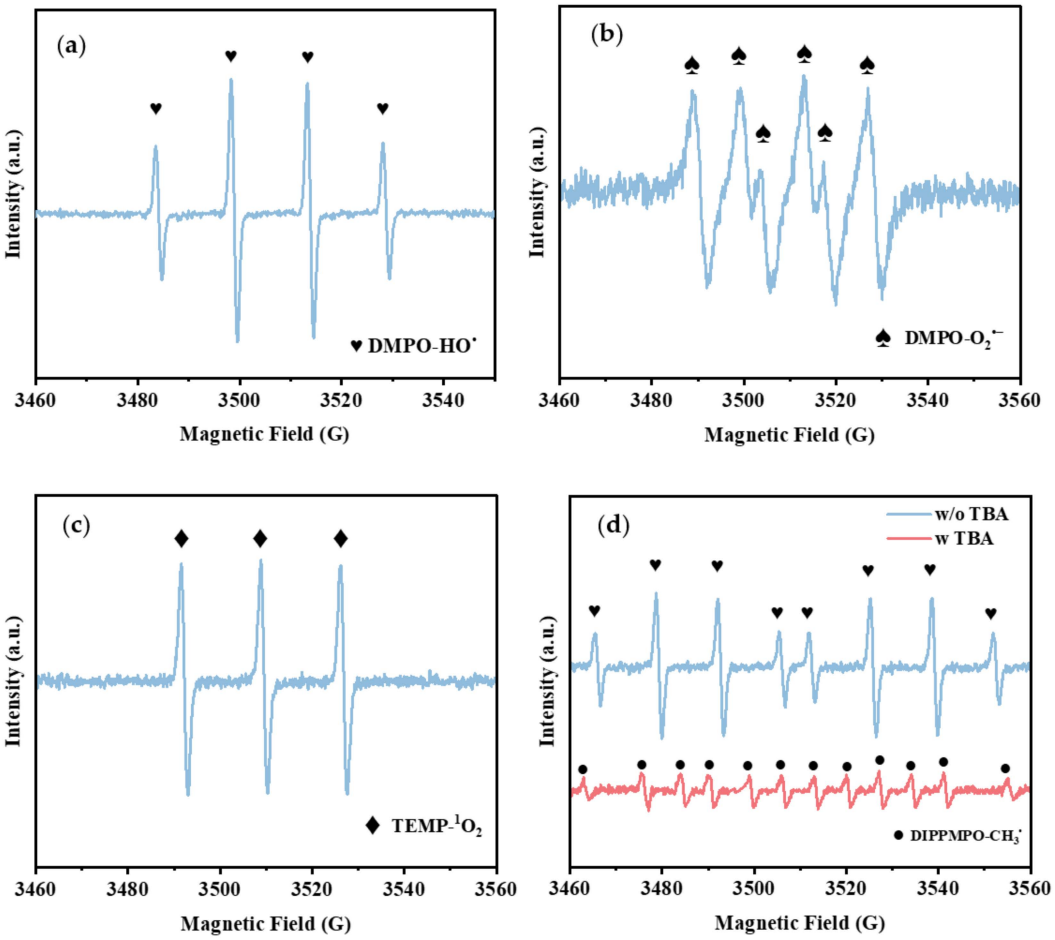

Figure 5. ESR spectra of (**a**) DMPO-$HO^{\bullet}$, (**b**) DMPO-$O_2^{\bullet-}$ with ethanol as solvent, (**c**) TEMP-$^1O_2$ and (**d**) DIPPMPO-$HO^{\bullet}$ and DIPPMPO-$CH_3^{\bullet}$ adducts without and with TBA.

The results of ESR spectra showed that $HO^{\bullet}$, $O_2^{\bullet-}$, $^1O_2$ and R-$O^{\bullet}$ were produced during the reaction. To further identify the role of ROSs, quenching experiments were designed. Owing to rapid reaction rate constants, isopropanol (IPA), chloroform ($CHCl_3$) and furfuryl alcohol (FFA) were chosen to quench $HO^{\bullet}$, $O_2^{\bullet-}$ and $^1O_2$. Based on the competitive reaction kinetics, the appropriate concentrations of scavengers were calculated and the results are discussed in Text S9. The experimental results of all selected scavengers are exhibited in Figure 6. When IPA was added, the degradation of SMX was significantly inhibited, which indicated a predominant contribution of $HO^{\bullet}$ to the system, approximately accounting for 73.3% of SMX degradation. The results of adding $CHCl_3$ suggested that $O_2^{\bullet-}$ had little contribution toward the degradation of SMX. Moreover, FFA need to be dissolved in MeOH to counteract its instability in the aqueous solution [46,56]. An equal concentration of MeOH was added to the reaction system as a control, and thus the difference between FFA and MeOH could be considered the actual contribution of $^1O_2$ to the degradation of SMX. In comparison to the impact of adding FFA and MeOH on the

degradation of SMX, it was evident that $^1O_2$ had almost no effect on the oxidative capability of the system.

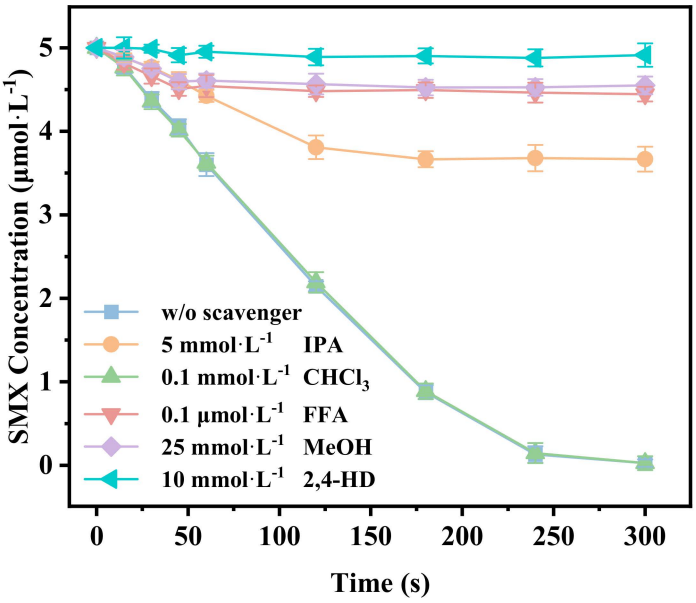

Figure 6. Effects of different scavengers on SMX degradation in FeS/PAA system. Experimental conditions: $[SMX]_0$ = 5 μmol·L^{-1}, $[FeS]_0$ = 50 mg·L^{-1}, $[PAA]_0$ = 200 μmol·L^{-1}, pH = 5.5.

According to Kim et al. [18], $Fe^{IV}O^{2+}$ could also be produced in the process of PAA activation by Fe(II) (Equation (15)). So, methyl phenyl sulfone ($PMSO_2$) generated from methyl phenyl sulfoxide (PMSO) was quantitated in order to understand the contribution of $Fe^{IV}O^{2+}$ in the FeS/PAA system (experimental conditions: $[PMSO]_0$ = 100 μmol·L^{-1}, $[FeS]_0$ = 50 mg·L^{-1}, $[PAA]_0$ = 200 μmol·L^{-1}, pH = 5.5). The results showed that the decomposition rate of PMSO was approximately 14.1% within 5 min, while almost no converted $PMSO_2$ followed, indicating the absence of $Fe^{IV}O^{2+}$ in FeS/PAA process. 2,4-hexadiene (2,4-HD) was also adopted in this paper considering its high reactivity with HO$^\bullet$ and R-O$^\bullet$. Figure 6 shows that SMX decomposition was greatly inhibited after adding 2, 4-HD, and the effect of HO$^\bullet$ and R-O$^\bullet$ was proven. So, the contribution ratio of R-O$^\bullet$ towards SMX elimination was about 26.7% by subtracting the results of IPA. In conclusion, the contribution of HO$^\bullet$ was relatively critical, while that of R-O$^\bullet$ was minor, and $^1O_2$, $O_2^{\bullet-}$ and $Fe^{IV}O^{2+}$ were hardly involved in the degradation.

$$CH_3C(O)OOH + Fe(II) \rightarrow CH_3C(O)OH + Fe^{IV}O^{2+} \quad (15)$$

3.6. Proposed Reaction Sites and Mechanism

The discussion above confirmed the strong oxidation capacity of the FeS/PAA system deprived from the activation of PAA by FeS. However, it was not entirely clear whether the reaction occurred on the surface of FeS or in the solution. This was because, during the reaction process of the FeS/PAA system, the iron element might leach into the solution. The Fe(II)/PAA homogeneous system showed great degradation ability towards organic compounds [5,18] as well. Therefore, it was necessary to evaluate the contribution of homogeneous PAA activation to SMX removal. Dissolved Fe(II) during the reaction was determined, and the result is depicted in Figure S10. Fe(II) concentration was moderately increase during the 2 min of the reaction, while it significantly surged subsequently, reaching around 100 μmol·L^{-1} at 5 min. In addition, 50 mg·L^{-1} FeS in the system was equivalent to approximately 573 μmol·L^{-1} Fe(II) in terms of moles. This indicated that the activation of PAA by leached Fe(II) was relatively slow in the early stages, followed by a

rapid enhancement, which corresponded to the trend of improved degradation efficiency of SMX in the system.

Xu et al. [57] pointed out that ionic strength could influence the outer-sphere interactions dominated by electrostatic bonds rather than the inner-sphere complexation (covalent bond and ionic bond). The change in ionic strength to SMX degradation efficiency was assessed by adding $NaClO_4$ to the reaction system. As reflected in Figure 7a, the decomposition of SMX was affected by different ionic strengths to some extent. The results showed strong inner-sphere interaction between FeS and other components, while inner-sphere complexation was weak. Furthermore, the F^- was relatively stable in terms of physicochemical properties and generally had no effect on the degradation of organic pollutants in homogeneous systems. Studies revealed that during the heterogeneous activation of PAA, surface-bound free radicals made great contributions to contaminant degradation [58]. Meanwhile, F^- in the solution could desorb $HO^•$ bound on a solid surface by forming a strong hydrogen bond (surface-bound $HO^•\cdots$F-particle) so as to ascertain whether $HO^•$ was generated on the surface [59]. Fe(III) in the solution could form the $[FeF_6]^{3-}$complex with F^-, and more details can be found in Text S10. In order to investigate the role of Fe(II) on the surface of FeS, NaF was added to the solution. It can be observed from Figure 7b that SMX removal was gradually inhibited with the increase in F^- concentration, indicating that the reaction sites on the surface of FeS were also involved in the process of PAA activation. Approximately 41.2% of SMX abatement was inhibited by 2.0 mmol·L^{-1} NaF solution, which was also regarded as the contribution of surface-bound Fe(II) on FeS material. In other words, the leached Fe(II) was responsible for the remaining 58.8% decomposition of SMX. On this basis, rapid removal for SMX in the selected system was attributed to the participation of both dissolved Fe(II) ions in the aqueous solution and surface-bound Fe(II) on FeS in PAA activation, with the former playing the major role.

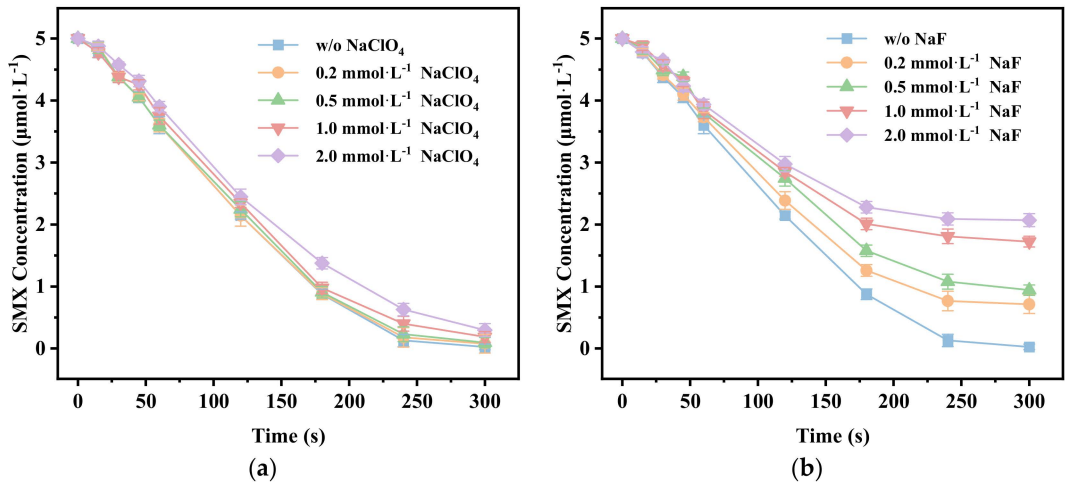

Figure 7. Effect of (**a**) $NaClO_4$ and (**b**) NaF on SMX degradation in FeS/PAA system. Experimental conditions: $[SMX]_0$ = 5 μmol·L^{-1}, $[FeS]_0$ = 50 mg·L^{-1}, $[PAA]_0$ = 200 μmol·L^{-1}, pH = 5.5.

3.7. Degradation Pathways and Toxicity Analysis of SMX

The degradation pathways of SMX in the FeS/PAA system were studied. Nine major intermediate compounds were identified by LC-QTOF-MS, and detailed information is shown in Table S5. Previous studies demonstrated the feasibility of frontier electron density (FED) theory in predicting reactive sites. To further predict the reactive sites of SMX, DFT and FED calculations were applied to clarify the atoms or sites where the SMX molecule was attacked by free radicals (Text S8 and Table S6) [37,60]. Figure S12 shows the molecular orbital diagrams of SMX. Following the results of instrumental analysis and theoretical calculation, five possible degradation pathways were proposed, as shown in Figure S13.

In general, organic compounds were vulnerable to react with ROS through addition reactions, hydrogen atom abstraction, and single-electron transfer (SET) [61]. The hy-

droxylation reaction corresponding to two pathways was as follows: The methyl group attached to the 14(C) atom was replaced by a hydroxyl group, resulting in the formation of hydroxylation P1 (Pathway I) [62]. Since the carbon atoms on the benzene ring had higher FED^2(HOMO) + FED^2(LUMO) values compared to other carbon atoms, SMX was also subject to hydroxylation to produce P2 via attack of $HO^{\bullet}$. The subsequent breakdown of γ bond of P2 occurred and was responsible for the subsequent generation of P3 and P4 (Pathway II). Additionally, the β, γ and δ bond of SMX were prone to cleavage due to ROS attack [63]. Based on the location of the bond breakage, three pathways were speculated to be involved. The formation of products P5 and P6 after the reaction suggested the existence of cleavage of β bond (Pathway III). SMX was oxidized to be broken at γ bond, and P7 and P8 were formed as a result (Pathway IV). Moreover, the detected intermediate compounds P9 and P4 were initially produced by the cleavage of the γ bond (Pathway V).

The toxicity of SMX and degradation intermediates produced during the SMX degradation process were evaluated via ECOSAR and the T.E.S.T. program (Tables S7 and S8). As illustrated in Figure S14, SMX possessed the lowest $lgLC_{50}$ of 0.81 for daphnid in comparison with other intermediates, implying that the acute toxicity of SMX was strongest and the virulence of most intermediates exhibited a significant decline (exclusive for P4 and P5). Similarly, an obvious decrease in chronic toxicity could be seen in the great majority of degradation intermediates, except for P4 and P5. Furthermore, the predicted result of almost all intermediates was developmental non-toxicity compared to SMX. The analysis above revealed that the toxicity of SMX was reduced during the degradation process, while potential toxicity still existed for certain degradation intermediates. Hence, in order to mitigate the toxicity, it was essential that the degradation time should be prolonged to ensure a complete decomposition of SMX into CO_2 and H_2O.

The TOC analyzer was applied to further explore the mineralization degree of the SMX/FeS/PAA system after the reaction. Figure S15 presents the TOC removal rate during FeS/PAA oxidation of SMX. The initial TOC value included the organic carbon both in SMX and PAA, and approximately 7.43% of TOC was abated after the 12 h reaction. The reason for the low TOC removal rate in this study can be found in Text S11. The results highlighted the strategy of prolonging the reaction time again.

4. Conclusions

In this study, FeS material was successfully synthesized, confirming the feasibility of improvement for activating PAA. In comparison with other activation materials, such as CuS and Fe_3O_4, FeS offered great benefits in PAA activation for SMX decomposition. The FeS/PAA process exhibited rapid degradation capability, achieving complete degradation of SMX within 5 min under optimal conditions, with a k_{obs} of 7.71×10^{-4} s^{-1}. In addition, the presence of H_2O_2 in the PAA fabricated solution had no effect on degradation. Although FeS could also activate other familiar oxidants, the degradation efficiency of the PAA activation process was much higher. A series of experiments including Fe(II) concentration determination and ion intensity alterations demonstrated that both dissolved Fe(II) ions and active sites on the surface of FeS participated in the activation process of PAA, thereby synergistically promoting the efficient degradation of SMX. Meanwhile, the FeS/PAA process was verified to demonstrate a better degradation capacity in acidic and neutral environments. The analysis of identified active species revealed that $HO^{\bullet}$ was the primary active species during the degradation of SMX in the FeS/PAA system, followed by the degradation performance of $R\text{-}O^{\bullet}$. Five possible degradation pathways were proposed. Overall, this study validated the oxidation potential of the FeS/PAA process and provided a promising strategy for refractory organic pollutant abatement in the future.

Supplementary Materials: The following supporting information can be downloaded at: https://www.mdpi.com/article/10.3390/w16172405/s1, Table S1: Experimental equipment; Table S2: Second-order rate constants for reactions between organics and reactive oxygen species (ROS) ($mol^{-1}\cdot s^{-1}$); Table S3: BET surface area, particle size, pore diameter and pore volume of FeS; Table S4: Comparison of pollutant degradation in PAA system activated by different heterogeneous catalysts; Table S5:

Possible structures of SMX degradation intermediates; Table S6: Front-line electron density (FED) values for each atom of SMX; Table S7: The ecotoxicity of SMX identified intermediates predicted by ECOASR; Table S8: The ecotoxicity of SMX identified intermediates predicted by T.E.S.T; Text S1: Chemicals; Text S2: Morphology and structure of synthesized FeS; Text S3: Preparation procedure of PAA; Text S4: Determination of PAA and H_2O_2 concentration; Text S5: Preparation and calibration of $KMnO_4$ solution; Text S6: Experimental devices; Text S7: DFT calculation; Text S8: Acute and chronic toxicity assessment; Text S9. The calculation of quenching agent concentration; Text S10. More details on the discussion of F^-; Text S11. The reason for the low TOC removal rate; Figure S1: SEM images of FeS at different magnification; Figure S2: High-resolution XPS spectrum of (a) Fe 2p, (b) S 2p for FeS; (c) XRD patterns and (d) N_2 adsorption–desorption isotherm curves of FeS; Figure S3: The pore-size distribution curves of FeS; Figure S4: The effect of the presence of 20 μmol·L^{-1} H_2O_2 in PAA tested solution on SMX degradation; Figure S5: Effect of (a) FeS dosage and (b) PAA concentration on their corresponding degradation rate constants in FeS/PAA system; Figure S6. Effect of SMX concentration on (a) SMX degradation and (b) corresponding degradation rate constants in FeS/PAA system; Figure S7. Effects of initial pH values on their corresponding degradation rate constants in FeS/PAA system; Figure S8. The real reaction pH value during FeS/PAA process; Figure S9. Distribution of PAA as function of pH; Figure S10. Time-dependent concentration of dissolved Fe(II) in FeS/PAA system; Figure S11. Residual PAA in the SMX/FeS/PAA system; Figure S12. (a) The optimized chemical structure of SMX molecular; (b) HOMO and (c) LUMO orbitals of SMX; Figure S13. The degradation pathways of SMX in FeS/PAA system; Figure S14. The (a) acute and (b) chronic toxicity of SMX and its TPs; Figure S15. The TOC removal rate during FeS/PAA oxidation of SMX.

Author Contributions: L.L.: experiments, data curation, writing—original draft, writing—review and editing. Y.W.: methodology, supervision, writing—review and editing. W.D.: methodology, writing—review and editing, funding acquisition. All authors have read and agreed to the published version of the manuscript.

Funding: This work was supported by the Foundation of Key Laboratory of Yangtze River Water Environment, Ministry of Education (Tongji University), China (No. YRWEF202101), and by the National Natural Science Foundation of China (No. NSFC 21607116).

Data Availability Statement: Data are contained within this article.

Acknowledgments: The authors are extremely appreciative of the teacher's advice and the assistance of the research group's pupils.

Conflicts of Interest: The authors declare no conflicts of interest.

References

1. Giannakis, S.; Lin, K.-Y.A.; Ghanbari, F. A review of the recent advances on the treatment of industrial wastewaters by Sulfate Radical-based Advanced Oxidation Processes (SR-AOPs). *Chem. Eng. J.* **2021**, *406*, 127083. [CrossRef]
2. Li, Y.; Dong, H.; Li, L.; Tang, L.; Tian, R.; Li, R.; Chen, J.; Xie, Q.; Jin, Z.; Xiao, J.; et al. Recent advances in waste water treatment through transition metal sulfides-based advanced oxidation processes. *Water Res.* **2021**, *192*, 116850. [CrossRef] [PubMed]
3. Wang, Z.P.; Chen, Z.B.; Li, Q.B.; Wang, J.W.; Cao, L.S.; Cheng, Y.J.; Yu, S.W.; Liu, Z.Z.; Chen, Y.Q.; Yue, S.Y.; et al. Non-radical activation of peracetic acid by powdered activated carbon for the degradation of sulfamethoxazole. *Environ. Sci. Technol.* **2023**, *57*, 10478–10488. [CrossRef]
4. Zhang, K.J.; Zhou, X.Y.; Du, P.H.; Zhang, T.Q.; Cai, M.Q.; Sun, P.Z.; Huang, C.H. Oxidation of β-lactam antibiotics by peracetic acid: Reaction kinetics, product and pathway evaluation. *Water Res.* **2017**, *123*, 153–161. [CrossRef] [PubMed]
5. Wang, Z.P.; Wang, J.W.; Xiong, B.; Bai, F.; Wang, S.L.; Wan, Y.; Zhang, L.; Xie, P.C.; Wiesner, M.R. Application of cobalt/peracetic acid to degrade sulfamethoxazole at neutral condition: Efficiency and mechanisms. *Environ. Sci. Technol.* **2020**, *54*, 464–475. [CrossRef] [PubMed]
6. Ao, X.-w.; Eloranta, J.; Huang, C.-H.; Santoro, D.; Sun, W.-j.; Lu, Z.-d.; Li, C. Peracetic acid-based advanced oxidation processes for decontamination and disinfection of water: A review. *Water Res.* **2021**, *188*, 116479. [CrossRef]
7. Cao, L.; Wang, J.; Wang, Z.; Yu, S.; Cheng, Y.; Ma, J.; Xie, P. Inactivation of Microcystis Aeruginosa by peracetic acid combined with ultraviolet: Performance and characteristics. *Water Res.* **2022**, *208*, 117847. [CrossRef]
8. Wang, Z.Y.; Shao, Y.S.; Gao, N.Y.; Xu, B.; An, N.; Lu, X. Comprehensive study on the formation of brominated byproducts during heat-activated persulfate degradation. *Chem. Eng. J.* **2020**, *381*, 10. [CrossRef]
9. Chen, F.; Liu, L.L.; Chen, J.J.; Li, W.W.; Chen, Y.P.; Zhang, Y.J.; Wu, J.H.; Mei, S.C.; Yang, Q.; Yu, H.Q. Efficient decontamination of organic pollutants under high salinity conditions by a nonradical peroxymonosulfate activation system. *Water Res.* **2021**, *191*, 13. [CrossRef]

10. Choong, Z.Y.; Lin, K.Y.A.; Lisak, G.; Lim, T.T.; Oh, W.D. Multi-heteroatom-doped carbocatalyst as peroxymonosulfate and peroxydisulfate activator for water purification: A critical review. *J. Hazard. Mater.* **2022**, *426*, 21. [CrossRef]
11. Li, R.B.; Manoli, K.; Kim, J.; Feng, M.B.; Huang, C.H.; Sharma, V.K. Peracetic acid-Ruthenium(III) oxidation process for the degradation of micropollutants in water. *Environ. Sci. Technol.* **2021**, *55*, 9150–9160. [CrossRef]
12. Liu, B.; Guo, W.; Jia, W.; Wang, H.; Zheng, S.; Si, Q.; Zhao, Q.; Luo, H.; Jiang, J.; Ren, N. Insights into the oxidation of organic contaminants by Co(II) activated peracetic acid: The overlooked role of high-valent cobalt-oxo species. *Water Res.* **2021**, *201*, 117313. [CrossRef]
13. Dong, J.; Xu, W.; Liu, S.; Gong, Y.; Yang, T.; Du, L.; Chen, Q.; Tan, X.; Liu, Y. Lignin-derived biochar to support $CoFe_2O_4$: Effective activation of peracetic acid for sulfamethoxazole degradation. *Chem. Eng. J.* **2022**, *430*, 132868. [CrossRef]
14. Zhu, E.Y.; Yuan, D.L.; Wang, Z.B.; Zhang, Q.R.; Tang, S.F. Insight into the activation mechanism of peracetic acid by molybdenum carbide for sulfamethoxazole decomposition. *Chem. Eng. J.* **2023**, *474*, 10. [CrossRef]
15. Chen, S.; Cai, M.; Liu, Y.; Zhang, L.; Feng, L. Effects of water matrices on the degradation of naproxen by reactive radicals in the UV/peracetic acid process. *Water Res.* **2019**, *150*, 153–161. [CrossRef]
16. Chen, J.Y.; Pan, H.J.; Chen, Y.L.; Zhou, Z.M.; Jing, G.H.; Zhao, X.D. Efficient activation of peracetic acid for abatement of tetracycline by W-doped CuS via regulating copper redox cycling. *Chem. Eng. J.* **2023**, *464*, 16. [CrossRef]
17. Kim, J.; Wang, J.Y.; Ashley, D.C.; Sharma, V.K.; Huang, C.H. Picolinic Acid-Mediated Catalysis of Mn(II) for Peracetic Acid Oxidation Processes: Formation of High-Valent Mn Species. *Environ. Sci. Technol.* **2023**, *57*, 18929–18939. [CrossRef] [PubMed]
18. Kim, J.; Zhang, T.Q.; Liu, W.; Du, P.H.; Dobson, J.T.; Huang, C.H. Advanced Oxidation Process with Peracetic Acid and Fe(II) for Contaminant Degradation. *Environ. Sci. Technol.* **2019**, *53*, 13312–13322. [CrossRef] [PubMed]
19. Wang, Q.; Zeng, H.; Liang, Y.H.; Cao, Y.; Xiao, Y.; Ma, J. Degradation of bisphenol AF in water by periodate activation with FeS (mackinawite) and the role of sulfur species in the generation of sulfate radicals. *Chem. Eng. J.* **2021**, *407*, 11. [CrossRef]
20. Shao, S.; Li, X.S.; Gong, Z.M.; Fan, B.; Hu, J.H.; Peng, J.B.; Lu, K.; Gao, S.X. A new insight into the mechanism in Fe_3O_4@CuO/PMS system with low oxidant dosage. *Chem. Eng. J.* **2022**, *438*, 11. [CrossRef]
21. Song, M.J.; Nguyen, Q.B.; Kim, C.; Hwang, I. Sustained activation of persulfate by slow release of Fe(II) from silica-coated nanosized zero-valent iron for in situ chemical oxidation. *Water Res.* **2023**, *246*, 11. [CrossRef]
22. Gong, Y.Y.; Tang, J.C.; Zhao, D.Y. Application of iron sulfide particles for groundwater and soil remediation: A review. *Water Res.* **2016**, *89*, 309–320. [CrossRef] [PubMed]
23. Chen, H.; Zhang, Z.L.; Mingbao, F.B.; Liu, W.; Wang, W.J.; Yang, Q.; Hu, Y.N. Degradation of 2,4-dichlorophenoxyacetic acid in water by persulfate activated with FeS (mackinawite). *Chem. Eng. J.* **2017**, *313*, 498–507. [CrossRef]
24. Xu, H.D.; Sheng, Y.Q. New insights into the degradation of chloramphenicol and fluoroquinolone antibiotics by peroxymonosulfate activated with FeS: Performance and mechanism. *Chem. Eng. J.* **2021**, *414*, 9. [CrossRef]
25. Fan, J.H.; Gu, L.; Wu, D.L.; Liu, Z.G. Mackinawite (FeS) activation of persulfate for the degradation of p-chloroaniline: Surface reaction mechanism and sulfur-mediated cycling of iron species. *Chem. Eng. J.* **2018**, *333*, 657–664. [CrossRef]
26. Xing, D.Y.; Shao, S.J.; Yang, Y.Y.; Zhou, Z.M.; Jing, G.H.; Zhao, X.D. Mechanistic insights into the efficient activation of peracetic acid by pyrite for the tetracycline abatement. *Water Res.* **2022**, *222*, 118930. [CrossRef] [PubMed]
27. Li, C.X.; Yuan, D.L.; Yang, K.; Wang, H.C.; Wang, Z.B.; Zhang, Q.R.; Tang, S.F. Reutilization of pyrite tailings in peracetic acid-based advanced oxidation process for water purification. *Sep. Purif. Technol.* **2024**, *354*, 129155. [CrossRef]
28. Liu, J.L.; Wong, M.H. Pharmaceuticals and personal care products (PPCPs): A review on environmental contamination in China. *Environ. Int.* **2013**, *59*, 208–224. [CrossRef] [PubMed]
29. Rout, P.R.; Zhang, T.C.; Bhunia, P.; Surampalli, R.Y. Treatment technologies for emerging contaminants in wastewater treatment plants: A review. *Sci. Total Environ.* **2021**, *753*, 17. [CrossRef] [PubMed]
30. Wang, A.B.; Guo, X.Y.; Morimoto, A.; Maetani, K.; Tanoue, R.; Tong-U-Dom, S.; Buranapratheprat, A. Transport and dilution of fluvial antibiotic in the Upper Gulf of Thailand. *Environ. Pollut.* **2021**, *288*, 10. [CrossRef] [PubMed]
31. Nawaz, M.; Shahzad, A.; Tahir, K.; Kim, J.; Moztahida, M.; Jang, J.; Alam, M.B.; Lee, S.H.; Jung, H.Y.; Lee, D.S. Photo-Fenton reaction for the degradation of sulfamethoxazole using a multi-walled carbon nanotube-$NiFe_2O_4$ composite. *Chem. Eng. J.* **2020**, *382*, 12. [CrossRef]
32. Lian, J.J.; Wang, H.L.; He, H.P.; Huang, W.L.; Yang, M.; Zhong, Y.; Peng, P.A. The reaction of amorphous iron sulfide with Mo(VI) under different pH conditions. *Chemosphere* **2021**, *266*, 10. [CrossRef]
33. Zhao, X.B.; Cheng, K.K.; Hao, J.B.; Liu, D.H. Preparation of peracetic acid from hydrogen peroxide, part II: Kinetics for spontaneous decomposition of peracetic acid in the liquid phase. *J. Mol. Catal. A-Chem.* **2008**, *284*, 58–68. [CrossRef]
34. Shen, P.; Hou, K.J.; Chen, F.; Pi, Z.J.; He, L.; Chen, S.J.; Li, X.M.; Yang, Q. Ultra-rapid and long-lasting activation of peracetic acid by Cu-Co spinel oxides for eliminating organic contamination: Role of radical and non-radical catalytic oxidation. *Chem. Eng. J.* **2023**, *463*, 13. [CrossRef]
35. Viollier, E.; Inglett, P.W.; Hunter, K.; Roychoudhury, A.N.; Van Cappellen, P. The ferrozine method revisited: Fe(II)/Fe(III) determination in natural waters. *Appl. Geochem.* **2000**, *15*, 785–790. [CrossRef]
36. Grimme, S.; Ehrlich, S.; Goerigk, L. Effect of the damping function in dispersion corrected density functional theory. *J. Comput. Chem.* **2011**, *32*, 1456–1465. [CrossRef]
37. Lu, T.; Chen, F.W. Multiwfn: A multifunctional wavefunction analyzer. *J. Comput. Chem.* **2012**, *33*, 580–592. [CrossRef] [PubMed]
38. Humphrey, W.; Dalke, A.; Schulten, K. VMD: Visual molecular dynamics. *J. Mol. Graph.* **1996**, *14*, 33–38. [CrossRef]

39. Tian, B.R.; Wu, N.N.; Liu, M.Z.; Wang, Z.Y.; Qu, R.J. Promoting effect of silver oxide nanoparticles on the oxidation of bisphenol B by ferrate(VI). *Environ. Sci. Technol.* **2023**, *57*, 15715–15724. [CrossRef] [PubMed]
40. Chen, H.; Zhang, Z.L.; Yang, Z.L.; Yang, Q.; Li, B.; Bai, Z.Y. Heterogeneous fenton-like catalytic degradation of 2,4-dichlorophenoxyacetic acid in water with FeS. *Chem. Eng. J.* **2015**, *273*, 481–489. [CrossRef]
41. Al-Anazi, A.; Abdelraheem, W.H.; Han, C.; Nadagouda, M.N.; Sygellou, L.; Arfanis, M.K.; Falaras, P.; Sharma, V.K.; Dionysiou, D.D. Cobalt ferrite nanoparticles with controlled composition-peroxymonosulfate mediated degradation of 2-phenylbenzimidazole-5-sulfonic acid. *Appl. Catal. B-Environ.* **2018**, *221*, 266–279. [CrossRef]
42. Zhang, H.X.; Li, C.W.; Lyu, L.; Hu, C. Surface oxygen vacancy inducing peroxymonosulfate activation through electron donation of pollutants over cobalt-zinc ferrite for water purification. *Appl. Catal. B-Environ.* **2020**, *270*, 10. [CrossRef]
43. Zhang, T.Q.; Huang, C.H. Modeling the kinetics of UV/peracetic acid advanced oxidation process. *Environ. Sci. Technol.* **2020**, *54*, 7579–7590. [CrossRef]
44. Cai, M.Q.; Sun, P.Z.; Zhang, L.Q.; Huang, C.H. UV/peracetic acid for degradation of pharmaceuticals and reactive species evaluation. *Environ. Sci. Technol.* **2017**, *51*, 14217–14224. [CrossRef] [PubMed]
45. Yang, Y.; Pignatello, J.J.; Ma, J.; Mitch, W.A. Comparison of halide impacts on the efficiency of contaminant degradation by sulfate and hydroxyl radical-based advanced oxidation processes (AOPs). *Environ. Sci. Technol.* **2014**, *48*, 2344–2351. [CrossRef]
46. Liu, H.H.; Zhao, J.; Wang, Y.; Wu, Y.L.; Dong, W.B.; Nie, M.H.; Wang, X.N. Enhancement of peroxymonosulfate activation by sinapic acid accelerating Fe(III)/Fe(II) cycle. *Chem. Eng. J.* **2022**, *446*, 8. [CrossRef]
47. Song, Z.; Zhang, Y.; Zhang, X.; Zhou, X.; Chen, Y.D.; Duan, X.G.; Ren, N.Q. Kinetics study of chloride-activated peracetic acid for purifying bisphenol A: Role of Cl_2/HClO and carbon-centered radicals. *Water Res.* **2023**, *242*, 8. [CrossRef]
48. Zhang, C.Q.; Brown, P.J.B.; Hu, Z.Q. Thermodynamic properties of an emerging chemical disinfectant, peracetic acid. *Sci. Total Environ.* **2018**, *621*, 948–959. [CrossRef]
49. Kim, J.; Du, P.H.; Liu, W.; Luo, C.; Zhao, H.; Huang, C.H. Cobalt/peracetic acid: Advanced oxidation of aromatic organic compounds by acetylperoxyl radicals. *Environ. Sci. Technol.* **2020**, *54*, 5268–5278. [CrossRef]
50. Yang, L.W.; She, L.H.; Xie, Z.H.; He, Y.L.; Tian, X.Y.; Zhao, C.L.; Guo, Y.Q.; Hai, C.; He, C.S.; Lai, B. Boosting activation of peracetic acid by Co@mZVI for efficient degradation of sulfamethoxazole: Interesting two-phase generation of reactive oxidized species. *Chem. Eng. J.* **2022**, *448*, 9. [CrossRef]
51. Fang, Z.Y.; Zhao, J.; Li, Y.; Wang, Y.; Qiu, T.; Wu, Y.L.; Dong, W.B.; Mailhot, G. Improving Fenton-like system with Catechin, an environmental-friendly polyphenol: Effects and mechanism. *Chem. Eng. J.* **2021**, *426*, 7. [CrossRef]
52. Li, G.B.; Huang, S.Q.; Zhu, N.W.; Yuan, H.P.; Ge, D.D. Near-infrared responsive upconversion glass-ceramic@BiOBr heterojunction for enhanced photodegradation performances of norfloxacin. *J. Hazard. Mater.* **2021**, *403*, 10. [CrossRef]
53. Finkelstein, E.; Rosen, G.M.; Rauckman, E.J. Spin trapping-Kinetics of the reaction of superoxide and hydroxyl radicals with nitrones. *J. Am. Chem. Soc.* **1980**, *102*, 4994–4999. [CrossRef]
54. Chalier, F.; Tordo, P. 5-Diisopropoxyphosphoryl-5-methyl-1-pyrroline N-oxide, DIPPMPO, a crystalline analog of the nitrone DEPMPO: Synthesis and spin trapping properties. *J. Chem. Soc.-Perkin Trans.* **2002**, *2*, 2110–2117. [CrossRef]
55. Rokhina, E.V.; Makarova, K.; Golovina, E.A.; Van As, H.; Virkutyte, J. Free Radical Reaction Pathway, Thermochemistry of Peracetic Acid Homolysis, and Its Application for Phenol Degradation: Spectroscopic Study and Quantum Chemistry Calculations. *Environ. Sci. Technol.* **2010**, *44*, 6815–6821. [CrossRef] [PubMed]
56. Li, Y.; Wu, Y.N.; Dong, W.B. Trace catechin enhanced degradation of organic pollutants with activated peroxymonosulfate: Comprehensive identification of working oxidizing species. *Chem. Eng. J.* **2022**, *429*, 7. [CrossRef]
57. Xu, Y.; Ai, J.; Zhang, H. The mechanism of degradation of bisphenol A using the magnetically separable $CuFe_2O_4$/peroxymonosulfate heterogeneous oxidation process. *J. Hazard. Mater.* **2016**, *309*, 87–96. [CrossRef] [PubMed]
58. Zhang, L.L.; Chen, J.B.; Zhang, Y.L.; Xu, Y.; Zheng, T.L.; Zhou, X.F. Highly efficient activation of peracetic acid by nano-CuO for carbamazepine degradation in wastewater: The significant role of H_2O_2 and evidence of acetylperoxy radical contribution. *Water Res.* **2022**, *216*, 10. [CrossRef] [PubMed]
59. Hou, X.J.; Huang, X.P.; Jia, F.L.; Ai, Z.H.; Zhao, J.C.; Zhang, L.Z. Hydroxylamine Promoted Goethite Surface Fenton Degradation of Organic Pollutants. *Environ. Sci. Technol.* **2017**, *51*, 5118–5126. [CrossRef]
60. Zhang, J.Y.; Zhao, R.X.; Cao, L.J.; Lei, Y.S.; Liu, J.; Feng, J.; Fu, W.J.; Li, X.Y.; Li, B. High-efficiency biodegradation of chloramphenicol by enriched bacterial consortia: Kinetics study and bacterial community characterization. *J. Hazard. Mater.* **2020**, *384*, 11. [CrossRef]
61. An, T.C.; Gao, Y.P.; Li, G.Y.; Kamat, P.V.; Peller, J.; Joyce, M.V. Kinetics and mechanism of $^{\bullet}$OH mediated degradation of dimethyl phthalate in aqueous solution: Experimental and theoretical studies. *Environ. Sci. Technol.* **2014**, *48*, 641–648. [CrossRef] [PubMed]

62. Gardner, D.V.; Howard, J.A.; Ingold, K.U. The inhibition of autoxidation by 2,4,6-tri-tert-butyl substituted phenol, aniline, and thiophenol. *Can. J. Chem.* **1964**, *42*, 2847–2851. [CrossRef]
63. Li, T.Y.; Ge, L.F.; Peng, X.X.; Wang, W.; Zhang, W.X. Enhanced degradation of sulfamethoxazole by a novel Fenton-like system with significantly reduced consumption of H_2O_2 activated by g-C_3N_4/MgO composite. *Water Res.* **2021**, *190*, 12. [CrossRef] [PubMed]